FINAL TECHNICAL REPORT

Fault Creep Dynamics, Earthquake Cycles and Earthquake Potential on the Hayward Fault: Collaborative Research with University of California, Berkeley and Indiana University

National Earthquake Hazard Reduction Program

U.S. Geological Survey

Award Numbers: **G09AP00097 and G09AP00103**

Term: July 1, 2009 – June 30, 2010

Principal investigator:

Roland Bürgmann

University of California, Berkeley
Department of Earth and Planetary Science
307 McCone Hall
Berkeley, CA 94720-4767
Telephone: (510) 643-9545;
Fax:(510) 643-9980;
e-mail: burgmann@seismo.berkeley.edu

Kaj M. Johnson
Indiana University
Dept. of Geological Sciences
1001 E. 10th St.
Bloomington, IN 47405-1405
812 855-3612 (tel.)
kajjohns@indiana.edu

Fault Creep Dynamics, Earthquake Cycles and Earthquake Potential on the Hayward Fault: Collaborative Research with University of California, Berkeley and Indiana University

Award Numbers: **G09AP00097 and G09AP00103**

Technical Abstract:

This investigation aimed to improve our understanding of the kinematics and dynamics of fault slip on the Hayward fault and its continuations to the north and south, with a focus on resolving where and when slip is accommodated seismically and aseismically. The Hayward fault is known to generate major M > 6.7 earthquakes, but currently creeps at 30-90% of its long-term slip rate along its surface trace. Recent research has focused on establishing the paleoseismic earthquake history of the fault, determining details of the fault geometry at depth from micro-seismicity, and resolving the depth and distribution of fault creep along the fault from kinematic inversions of geodetic measurements and repeating micro-earthquakes. In this new work, new data constraints and modeling of the dynamics of aseismic fault slip have allowed us to illuminate the role of fault creep in the timing, nature and magnitude of large Hayward fault ruptures. We used newly acquired InSAR satellite data to improve estimates of the distribution and extent of locked asperities along the fault. A discontinuity in these observed surface velocities indicates that the fault undergoes shallow aseismic creep. Using kinematic and mechanical elastic models, we relate the surface deformation pattern to the distribution of creep on the fault at depth. We infer that ~20% of the fault surface is not creeping, and is instead locked and accumulating elastic strain. A contemporary rupture of this locked fault region would result in a M~6.7 earthquake. The estimates help form the basis of more detailed dynamic rupture and ground motion model scenarios. We also developed spring-slider and 3D finite fault rate-state friction models of transient creep responses on the Hayward fault to sudden stress changes and compared with surface creep rate changes observed following the 1989 Loma Prieta earthquake. The state (healing) term in the friction law is critical for reproducing the observed evolution of surface creep; a popular simplified rate-dependent friction law is insufficient. Our results suggest that the creep event at the southern end of the Hayward fault extended to a depth of ~4 - 7.5km, consistent with our slip inversion results. The inferred critical slip distance, d_c, is 1-2 orders of magnitude larger than lab values and inferred $a\sigma$ values imply low effective fault-normal stresses of 5-30 MPa. This range of effective normal stress and inversion results for $(a-b)\sigma$ imply very small values for $a-b$ of 10^{-5} to 10^{-3}, smaller than typical lab values of order 10^{-3} to 10^{-2}. Earthquake simulations with such small $a-b$ values show that creeping areas on the Hayward fault may rupture during earthquakes.

Non-technical Abstract:

This investigation aimed to improve our understanding of the kinematics and dynamics of fault slip on the Hayward fault and its continuations to the north and south, with a focus on resolving where and when slip is accommodated seismically and aseismically. The Hayward fault is known to generate major M > 6.7 earthquakes, but currently creeps at 30-90% of its long-term slip rate along its surface trace. In this new work, new data constraints and modeling of the dynamics of aseismic fault slip have allowed us to illuminate the role of fault creep in the timing, nature and magnitude of large Hayward fault ruptures. We used newly acquired geodetic data to improve models of the distribution and extent of locked asperities along the fault. We infer that ~20% of the fault surface is not creeping, and is instead locked and accumulating elastic strain. A contemporary rupture of this locked fault region would result in a M~6.7 earthquake. The estimates help form the basis of more detailed dynamic rupture and shaking model scenarios. We also developed numerical models of the transient creep response observed on the Hayward fault due to sudden stress changes on the fault following the 1989 Loma Prieta earthquake. The modeling work allowed us to infer frictional properties on the fault and compare with laboratory values. The models suggest low effective fault-normal stresses of 5-30 MPa, indicating that the fault is weak. This range of effective normal stress, σ, and inversion results for a friction parameter $\sigma(a-b)$, that controls the stability of sliding on the fault, imply very small values for $a-b$ of 10^{-5} to 10^{-3}, smaller than typical lab values of order 10^{-3} to 10^{-2}. Our earthquake simulations with such small $a-b$ values show that creeping areas on the Hayward fault may be able to rupture during earthquakes which has important implications for the size of future earthquakes on the Hayward fault.

1. Distribution of locked asperities on the Hayward fault inferred from InSAR data and boundary element models

1.1 Summary

We use Permanent Scatterer InSAR (PSInSAR) measurements from multiple satellite viewing geometries and GPS data to measure the surface deformation associated with the Hayward fault in California. A discontinuity in these observed surface velocities indicates that the fault undergoes shallow aseismic creep; using kinematic and mechanical elastic models, we relate the surface deformation pattern to the distribution of creep on the fault at depth. We infer that ~20% of the fault surface is not creeping, and is instead locked and accumulating elastic strain. A contemporary rupture of this locked fault region would result in a M~6.7 earthquake.

1.2 Introduction

The Hayward fault accommodates strain in two different ways – in large (M~7) earthquakes, and by aseismic creep. In combination with its northern extension, the Rodgers Creek fault, it is currently considered the most dangerous fault in northern California [*UCERF*, 2008]. The presence of creep is important in terms of the potential for and distribution of strong ground motions in future earthquakes – areas that undergo creep dissipate strain that may otherwise be released seismically. It is also significant in terms of its direct effect on the surface, causing detectable and ongoing deformation and damage. Here we demonstrate that a spatially dense dataset of surface deformation rates, generated from advanced processing of satellite radar images, enables us to map out which areas of the fault are creeping – and also, therefore, which areas are locked and accumulating strain for the next major earthquake [*Funning et al.*, The source of major earthquakes on the Hayward fault, California, Geophysical Research Letters, in review, (2010).].

The northwestward motion of the Pacific plate with respect to California's Great Valley imposes a shear of ~38 mm/yr across the San Francisco Bay Area. Approximately 25% of this is accommodated by the Hayward fault [*d'Alessio et al.*, 2005]. In 1868, a M~6.8 earthquake, the last such on the fault, displaced the ground ~1.9 m [*Yu and Segall*, 1996] and caused extensive building damage along the eastern margin of San Francisco Bay, and in San Francisco itself [*Boatwright and Bundock*, 2008]; a repeat today could imperil a regional population of 7 million, both directly through building damage and indirectly through failure of lifelines that cross the fault. Paleoseismic studies show that the past five earthquakes on the fault have a mean repeat period of 138 ± 58 years [*Lienkaemper and Williams*, 2007], equal, within uncertainty, to the time elapsed since the 1868 earthquake, drawing a sharp focus on the need to prepare today for the next event and to estimate its potential location and effects.

Creep on the Hayward fault was first discovered around 40 years ago through identification of offset cultural features [*Cluff and Steinbrugge*, 1966; *Blanchard and Laverty*, 1966]. Motion at the surface trace of the fault is sufficiently rapid that it can be detected geodetically. Repeat cross-fault short baseline theodolite measurements over the past 30 years find a surface creep rate that varies along the fault between 3 and 8 mm/yr [*Lienkaemper et al.*, 2001; *McFarland et al.*, 2009]. In order to assess the spatial extent and rate at which this creep

occurs at depth it is necessary to measure surface velocities at high spatial resolution and at a range of distances either side from the fault trace. Existing GPS and Interferometric Synthetic Aperture Radar (InSAR) measurements [*d'Alessio et al.*, 2005; *Schmidt et al*., 2005] are limited in this regard, due to the expense of monitoring a sufficiently dense array of GPS sites on the ground and extensive vegetation cover east of the fault, respectively.

1.3 InSAR Data and Approach

A solution to this problem of limited coverage is to apply an advanced processing methodology to the existing satellite radar data. The Permanent Scatterer InSAR (PSInSAR) technique [*Ferretti et al.*, 2001] has been demonstrated to increase both the general precision of surface range-change velocity estimates and the spatial density of observation points, particularly in challenging (e.g. vegetated) terrains. The PSInSAR algorithms identify pixels on the ground that scatter radar stably over decades, thus maximizing the number of radar images that can be used, and use spatial and temporal filters to separate the phase signal due to deformation (which is temporally correlated) from that due to tropospheric noise (which is spatially, but not temporally correlated). The resulting data set gives a displacement time series and best linear velocity for each stable pixel, with tropospheric effects mitigated.

We use, in this way, radar imagery from three different satellite image frames – one 49-image dataset spanning 1992–2000, and a second 30-image dataset spanning 1992–2001, acquired using the European Space Agency ERS satellites in a descending orbit viewing geometry, and 46 images acquired by the Canadian Space Agency RADARSAT platform between 1998 and 2006 in an ascending viewing geometry. The difference in viewing geometry between the datasets, with the ERS data recording eastward motion as positive line-of-sight velocity (towards the satellite) and the RADARSAT data recording the same motion as negative line-of-sight velocity (away from the satellite), but both datasets recording subsidence as negative line-of-sight velocity, permits discrimination between horizontal and vertical deformation signals.

An abrupt change in range-change velocity can be seen at the mapped trace of the Hayward fault in all datasets (Figure 1.1b,c,d). The opposite sense of this velocity step in the different viewing directions is consistent with predominantly horizontal (strike-slip) motion across the fault. The magnitudes of these steps in velocity vary along the trace of the fault, reflecting along-strike variation in the surface creep rate. Simple geometric inversions of the velocity steps estimated at 5 km intervals along the fault trace , give a surface creep rate profile indistinguishable within error from that estimated from contemporaneous theodolite measurements [*Lienkaemper et al.*, 2001; *McFarland et al.*, 2009] or, where sufficiently dense, GPS data [*d'Alessio et al.*, 2005].

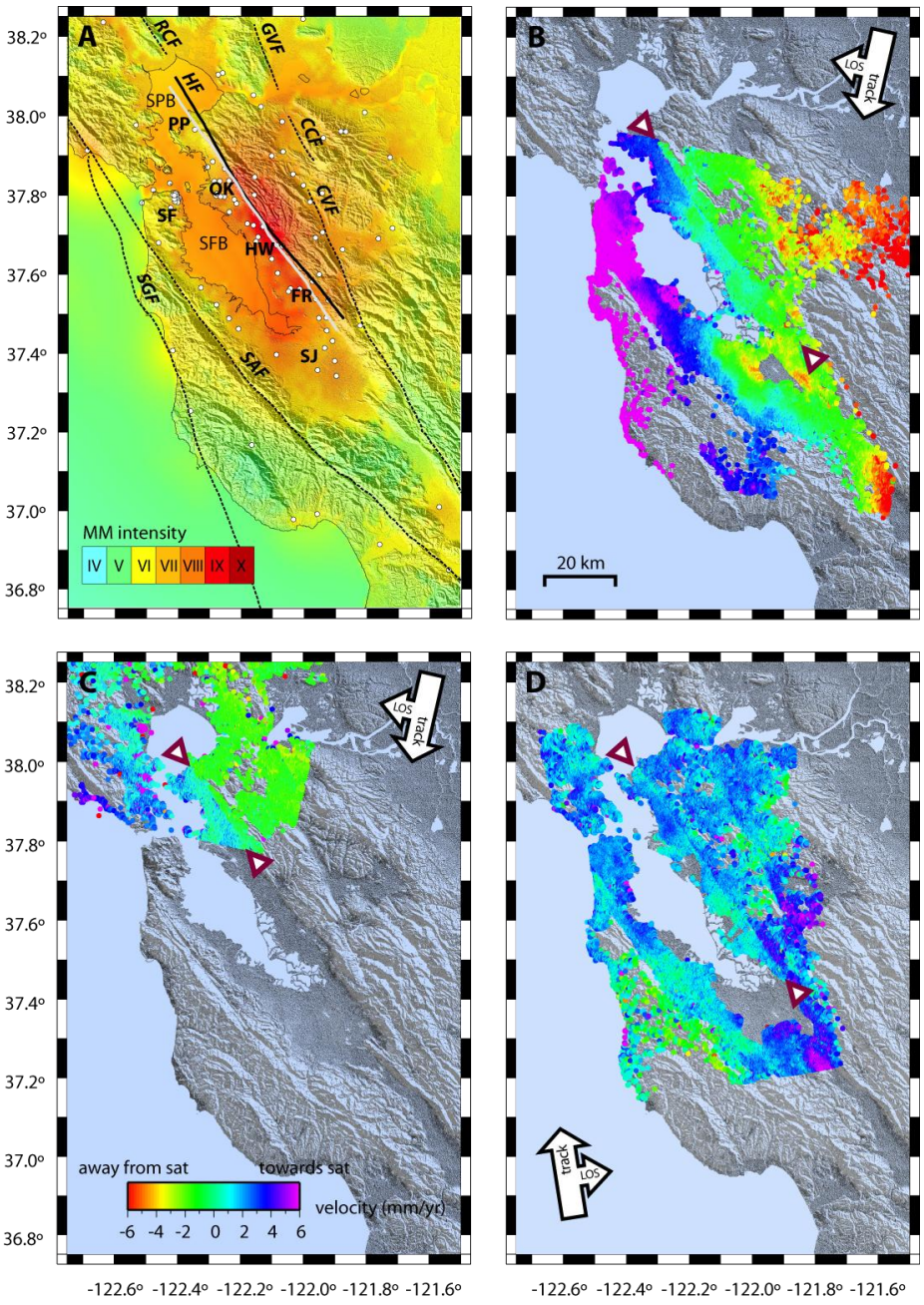

Figure 1.1: A) Regional fault locations and Modified Mercalli Intensity map (after Boatwrighgt and Bundock, 2009) of the 1868 Hayward earthquake. The Hayward fault is delimited by two solid lines – gray (fault surface trace), and black (base of the fault at 12 km depth); surface traces of other major faults indicated by dashed lines. White circles indicate the locations of intensity observations used to construct the map. Highest intensities from the 1868 event (VIII < MMI < X) are located either side of the Hayward fault in a zone extending from Oakland to Fremont, the area most likely to have ruptured in the earthquake. B) ERS descending track 70 PS-InSAR velocities for the interval 1992-2000. C) ERS descending track 342 PS-InSAR velocities for the interval 1992-2001. D) RADARSAT ascending track 38 PS-InSAR velocities for the interval 1998-2006. Creep on the Hayward fault is manifest as a step in velocity between 0.5 and 2 mm/yr in satellite line of sight (LOS) across a linear trend indicated by arrowheads. The sense of this velocity step is opposite in the ascending and descending datasets, indicating predominantly horizontal deformation. [HF – Hayward fault, SAF – San Andreas fault, RCF – Rodgers Creek fault, CVF – Calaveras fault, GVF – Green Valley fault, CCF – Concord fault; PP – Point Pinole, OK – Oakland, HW – Hayward, FR – Fremont, SF – San Francisco, SJ – San Jose; SPB – San Pablo Bay, SFB – San Francisco Bay]

1.4 Modeling

In order to place constraints on the area of the Hayward fault that is frictionally locked, we use a boundary element model methodology [*Thomas*, 1992], using a triangular element fault geometry fitted to microseismicity [*Schmidt et al*., 2005] and solving for the rate of slip on each element. The modeling is accomplished in two stages: first, a kinematic inverse model of slip is calculated via a smoothed non-negative least-squares inversion. Deep, semi-infinite dislocations were used beneath the locked zones of the major regional strike-slip faults in order to account for the regional strain accumulation on those structures. Second, a mechanically-coupled model, in which the elements of the Hayward fault are either considered locked (zero displacement) or creeping (zero shear traction) and are driven by the deep dislocation slip estimated in the kinematic model, was used to estimate the dimensions of areas on the fault that are fully locked .

Our kinematic model (Figure 1.2a) shows creep between 3 and 9 mm/yr over the majority of the fault plane. At the northwestern and southeastern ends of the fault, creep extends over the full width of the model fault at rates > 6 mm/yr; the highest surface rates are located in the upper 3 km of the fault in the vicinity of the city of Fremont, as seen in independent creepmeter data [*Bilham et al.*, 1998]. Over a 40 km-long zone extending from Oakland (in the NW) to Union City (in the SE), a low creep (< 1 mm/yr) zone is inferred, at depths of 4–12 km. We believe that this represents an area of the fault that is locked and accumulating significant elastic strain, and which may rupture in a future earthquake. A second area of low creep is found along the northernmost section of the fault, an area of limited microseismicity and thus likely fault locking [*Waldhauser and Schaff*, 2009]; however, we cannot confidently resolve details along this portion of the fault in our model, as it is covered by the waters of San Pablo Bay.

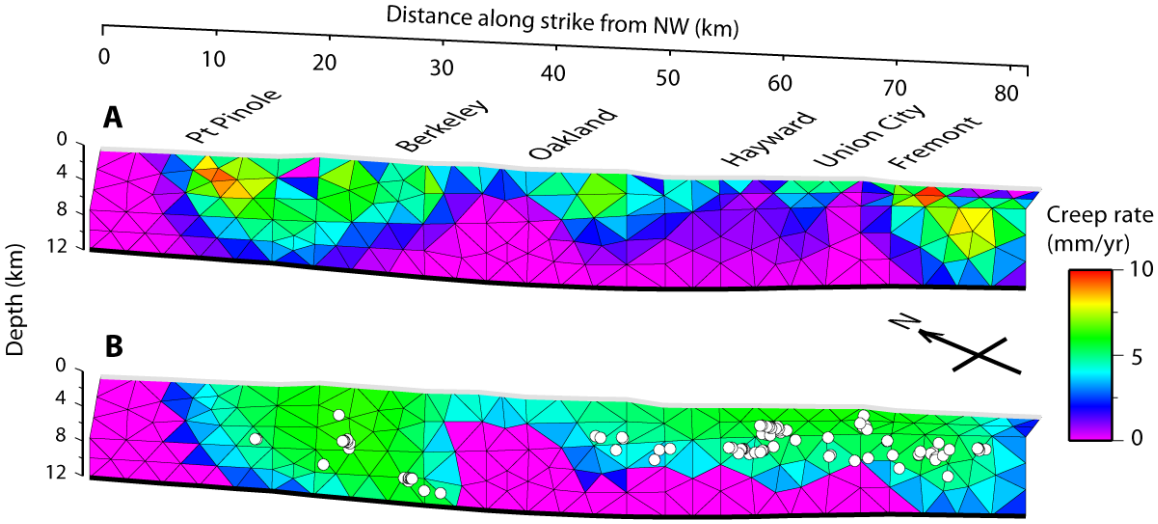

Figure 1.2: Kinematic and mechanical creep models of the Hayward fault that best fit the PS-InSAR and GPS data. The three-dimensional model fault geometry is shown from a vantage point perpendicular to average fault strike. Locations of cities mentioned in the text are shown. Triangles indicate individual fault elements. Gray line indicates surface trace, black line the bottom edge of the fault. A) Kinematic model of right-lateral fault creep. Magenta areas indicate portions of the fault that are not creeping. B) Mechanical model of fault creep. White circles are the locations of characteristic repeating earthquakes, which may indicate creep. Repeating earthquake locations and fault element locations after Schmidt et al., 2005.

Using the low-creep patches from the kinematic model as a starting point, we then systematically lock surrounding areas of the fault until the best match to the pattern of surface displacements is found. Our preferred mechanically-coupled model thus obtained (Figure 1.2b) has a 40 km-long locked zone, consistent with the length of the area of heaviest damage in the 1868 earthquake [Figure 1.1a] and covering approximately 20% of the fault surface above 12-km depth. In the vicinity of Oakland, where creep rates are lowest, the locked patch extends from the base of the model fault to within 4 km of the surface, as inferred in earlier studies considering surface creep [*Simpson et al.*, 2001; *Malservisi et al.*, 2003]; elsewhere the locked zone extends up to a depth of 6 km. The locked zone approximately matches the dimensions of a mapped, mechanically strong greywacke unit thought to be located along the west face of the fault surface [*Graymer et al.*, 2005], however no obvious correlation between lithology and fault behavior can be inferred for the creeping areas.

1.5 Discussion and Conclusions

Assuming that the deep dislocation loading rate of 9.5 mm/yr that we use in our modeling is applicable over the full interseismic interval on the Hayward fault and a crustal rigidity of 30 GPa, we infer that the locked zone is accumulating a seismic moment deficit equivalent to a Mw 6.5 earthquake per century. A contemporary repeat of the 1868 earthquake would thus be a Mw $\geq$ 6.7 event. An example of the potential ground motions for such an event is shown in Figure 1.3. In this particular scenario, bilateral rupture causes intense shaking (MMI VIII-IX) at either end of the locked zone. More asymmetric patterns of shaking, with concentrations of damage in the northwest or southeast can be generated depending on the location of the hypocenter with respect to the locked zone and resulting directivity effects [*Aagaard et al.*, 2010 a, b].

This scenario places a lower bound on potential ground motions, as the behavior of the creeping areas of the Hayward fault during seismic rupture is not known – all of these areas creep at rates lower than the loading rate, suggesting that they, too are accumulating a moment deficit, albeit at a slower rate than the locked zone. If the earthquake rupture were able to propagate into the creeping areas, the seismic moment release, and thus magnitude, would be greater. If the slip deficit on the currently creeping fault surface is made up during the next Hayward fault earthquake, the expected magnitude of the event would M 6.7.

Geodetic data from the Parkfield segment of the San Andreas fault suggest that areas of fault creep and earthquake slip have remained spatially separate over the past two earthquake cycles [Murray and Langbein, 2006], with the creeping areas experiencing accelerated postseismic afterslip in the days following the 2004 Mw 6.0 earthquake [Johanson et al., 2006; Johnson et al., 2006]. The surface rupture measured by creepmeters was solely by aseismic afterslip that initiated in the hours following the earthquake [Langbein et al., 2006]. If this behavior holds for other partially creeping faults, such as the Hayward, we would expect slip in a future Hayward earthquake to be confined to the locked zone, with significant shallow afterslip in the shallow creeping zone in the days following the earthquake, that could pose an ongoing threat to cross-fault lifelines.

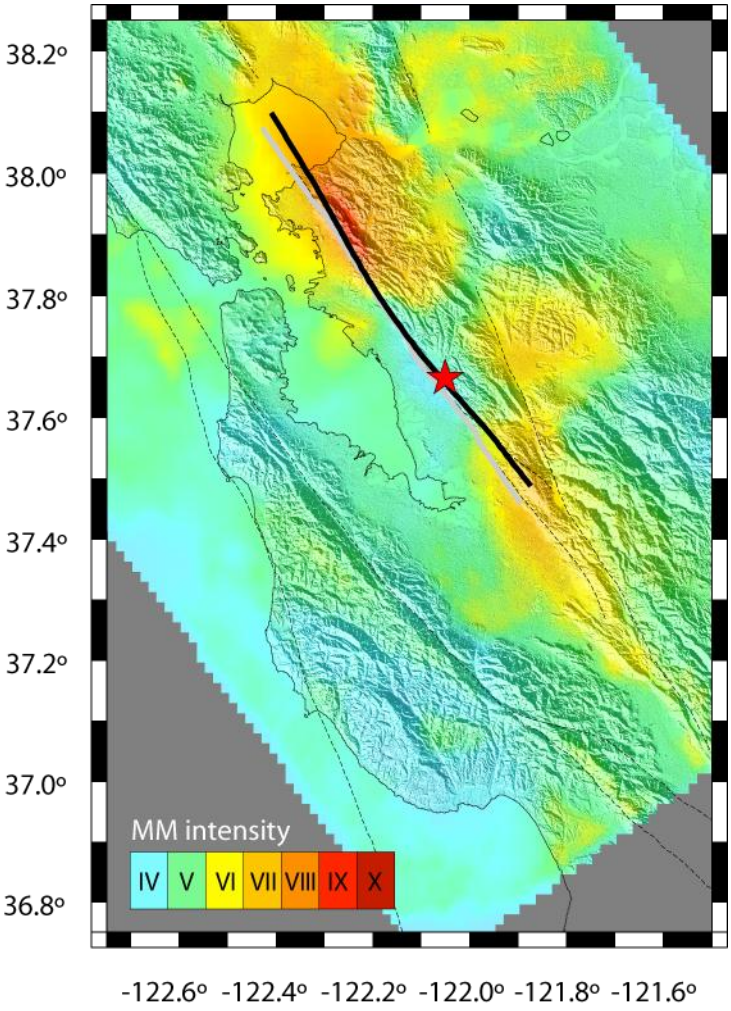

Figure 1.3: Predicted ground motion (Modified Mecalli) intensities for an earthquake scenario involving rupture of the locked zone identified in our mechanical model [Aagaard et al., 2010a b]. In this particular model, the rupture initiates in the center of the locked zone (the epicenter is marked by a red star) and ruptures bilaterally, creating elevated damage on either side along strike.

1.6 Data Availability

InSAR data collected by the ERS spacecraft used in this project have been obtained from the European Space Agency (ESA) and RADARSAT-1 data from the Alaska SAR facility (ASF). Much of these can be obtained via the WINSAR archive at UNAVCO. Inquiries for PS velocities and time series for research purposes can be made to Roland Bürgmann.
Data from GPS campaigns are publicly available from the UNAVCO Campaign Data Holdings Archive. Both raw GPS data and accompanying metadata are included and freely accessible at http://facility.unavco.org/data/gnss/campaign.php. Data collected by our group for this project are archived under the PI Name (Burgmann) for campaigns named “Calaveras Fault”, “Hayward Fault” and “Loma Prieta.”
Please see http://www.unavco.ucar.edu/data_support/data/general.html for policies regarding the use of these freely available data. Additional data used in this study included RINEX format files obtained from the U.S. Geological Survey and the Bay Area Regional Deformation Network

(BARD). These files include campaign-style surveying (USGS) and continuous GPS stations (BARD) and are available at the NCEDC at UC Berkeley.
Processed GPS solutions, including the BAVU velocity field, time series and GAMIT-format solution files (h-files) are available via the BAVU web pages at:

http://seismo.berkeley.edu/~burgmann/RESEARCH/BAVU/
http://seismo.berkeley.edu/~dalessio/BAVU/FILES/gamit.html

For more information regarding data availability, contact:

Dr. Roland Bürgmann
Department of Earth and Planetary Science, University of California, Berkeley
307 McCone Hall, Berkeley, CA 994720-4767
e-mail:burgmann@seismo.berkeley.edu
URL:http://www.seismo.berkeley.edu/~burgmann

2. Numerical models of transient fault creep on the southern end of the Hayward fault.

2.1 Summary

Theodolite measurements across the right-lateral Hayward fault, San Francisco Bay, California show a dramatic reduction in surface creep rate from 5-10 mm/yr before the 1989 Loma Prieta earthquake to nearly zero creep rate after the earthquake. A ~6-year period of nearly zero surface creep was followed by a sudden creep event that accumulated about 20-25 mm of right-lateral displacement followed by an eventual return to a steady creep by year ~2000. This creep behavior can be explained as a result of a sudden shear stress reduction on the fault and is consistent with predictions of models of a fault imbedded in an elastic medium with slip governed by laboratory-derived friction laws. We infer friction parameters on the fault using spring-slider and a boundary element models with the rate- and state-dependent friction laws. The state (healing) term in the friction law is critical for reproducing the observed evolution of surface creep; a popular simplified rate-dependent friction law is insufficient. Results suggest that the creep event extended to a depth of ~4 - 7.5km. The inferred critical slip distance, d_c, is 1-2 orders of magnitude larger than lab values and inferred $a\sigma$ values imply low effective fault-normal stresses of 5-30 MPa. This range of effective normal stress and inversion results for $(a-b)\sigma$ imply very small values for $a-b$ of 10^{-5} to 10^{-3}, smaller than typical lab values of order 10^{-3} to 10^{-2}. Earthquake simulations with such small $a-b$ values show that creeping areas on the Hayward fault may rupture during earthquakes.

2.2 Transient creep event

Creep measurements from 1980 to 2009 along the southern section of the Hayward fault show that the fault had been creeping at the surface at a nearly steady rate of 3.5-9 mm/yr before the creep behavior was modified by the 1989 Loma Prieta Earthquake on the San Andreas Fault [*Lienkaemper et al.,* 1997]. Small aperture survey measurements across the Hayward fault shown in Figure 2.1 indicate that the southern section of the fault essentially stopped creeping or even reversed sense of creep for about 6 years following the earthquake after which it exhibited a rapid transient creep event accumulating an average of 20-25 mm of displacement on the fault followed by a gradual return to steady creep around year 2000. Lienkaemper et al., [1997] suggested that the change in creep across the Hayward fault resulted from a reduction of right-lateral shear stress on the southern section of the fault due to the 1989 earthquake. Figure 2.2 shows the shear and normal stress changes on the Hayward fault computed from an elastic dislocation model by Lienkaemper et al. [1997]. Lienkaemper et al., [1997] suggested the 6-7 year duration of reduced creep rate and the inferred interseismic stressing rate on the fault is consistent with the time required to recover the static coseismic stress reduction on the fault. However, the reduction in stress alone cannot explain the temporal and spatial evolution of the creep evolution observed on the fault. Using numerical simulations, Schmidt and Bürgmann [2008] showed that a spring-slider model with a rate- and state- dependent friction law can explain the general pattern of nearly zero creep for ~6 years after the Loma Prieta earthquake followed by an abrupt recovery of the deficit in slip and a return to steady sliding.

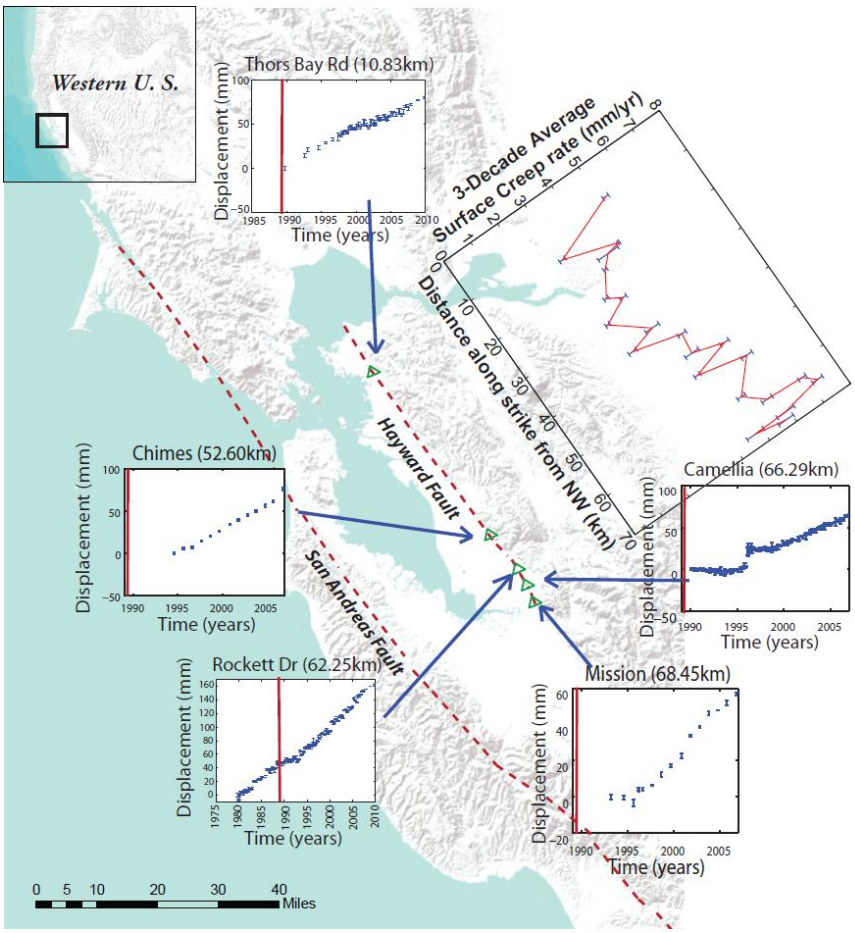

Figure 2.1: Tectonic structure of the San Francisco Bay Area and creep measurements from http://quake.wr.usgs.gov/docs/deformation/hfcreep/. *The plot parallel to the Hayward fault shows average surface creep rate from ~3 decades of measurements. Selected plots of the cumulative fault creep at stations shown with green triangles (Vertical red lines mark the time of the 1989 Loma Prieta Earthquake). Inset: Topography of the Western US.*

The purpose of this work is 1. Describe the temporal and spatial creep evolution across the southern section of the Hayward fault during the 1989-2007 time period, 2. Estimate the frictional parameters in the rate- and state- dependent friction law, 3. Estimate the effective normal stress, and 4. Estimate the depth extent of aseismic creep. To accomplish these, we model the transient creep using spring-slider and finite-fault numerical simulations with rate-state friction. We use the spring-slider model and Monte Carlo inversion methods to obtain posterior probability distributions of model parameters including the rate-state friction parameters and the area of the creeping part of the fault. We also develop a model for creep on a planar fault in an elastic half space using a boundary element formulation and compare the creep evolution with the spring-slider model and the creep data.

2.3 Spring-slider models

A spring-slider model is used in this study to explain the temporal evolution of the creep on the southern section of the Hayward fault between 1989 and 2007 and for inverting for

frictional parameters of the fault. The model consists of three sliders connected by springs and pulled at a steady rate. We adopt three sliders to represent distinct creep response in three sections of our study. For example, as illustrated in Figure 2.1, creep measurements at the northern end of our study area near Chimes display little or no transient creep response. Measurements in the central section of our study area near Camellia show the strongest response with a dramatic decrease in creep rate followed by a rapid accelerated creep recovery. Measurements in the southern section of our study area, near Mission, show a much smaller transient response. The three sliders allow for different model conditions and surface creep evolution within the three distinctive creep sections of the fault. The sliders are connected in a series arrangement with springs of stiffness, k_{int}, with each of the sliders tied to another spring, k, which is pulled at a far-field loading rate, *v*. Movement of the sliders is assumed to be governed by a rate- and state-dependent friction law [*Dieterich,* 1979a*; Ruina,* 1983]. Stress changes (both shear and normal stress) are imposed on the spring-slider system at t = 0, which represents the stress change on the fault resulting from the 1989 Loma Prieta earthquake. Shear and normal components of stress change are applied as an instantaneous stress step, and were extrapolated from the Post-Loma Prieta coulomb stress change on Hayward fault calculated by Lienkaemper et al., [2001]. The rate-state friction law states that the shear stress, τ, is dependent on sliding velocity, *v*, and a state variable, θ as

$$\tau = \left[\mu^* + a \ln \frac{v}{v_0} + b \ln \frac{\theta v_0}{d_c} \right] \sigma_{e0}, \qquad 1$$

where, μ* and v_o are reference values of frictional coefficient and velocity, respectively, $\sigma_{e0} = (\sigma - p)$, is the effective normal stress (where p is pore pressure), θ, is a state variable which represents the average lifetime of the asperity, d_c, is the critical slip distance over which the state variable evolves (it is the slip distance taken for the sliding surface to renew the asperity contact population, evolving between two steady states) and *a* and *b* are empirical constants. The time evolution of the state variable assuming a constant normal stress is given by the aging law,

$$\frac{d\theta}{dt} = 1 - \frac{\theta v}{d_c} \quad . \qquad 2$$

2.4 Spring-slider inversion results

The model parameters for the fault are estimated using the Monte Carlo Metropolis algorithm [*Fukuda et al,* 2009]. We invert for all the model parameters during the inversion process, except for the critical distance, d_c. It turns out that parameters are highly correlated with dc and it is difficult to invert jointly for d_c with other parameters. We therefore fix d_c and solve for other parameters. Friction parameters $a\sigma$ and $(a-b)\sigma$ are allowed to have different values on each slip patch. This is motivated by the fact that previous studies show that some of the information we are resolving, such as the extent of surface creep on the fault, the surface slip rate, etc, might be varying along the fault section. In summary, we have a total of eleven unknowns, d_c, l, $a\sigma_i$, $(a-b)\sigma_i$, and v_i where l is the patch dimension and $i=1,2,3$ represents the patch number.

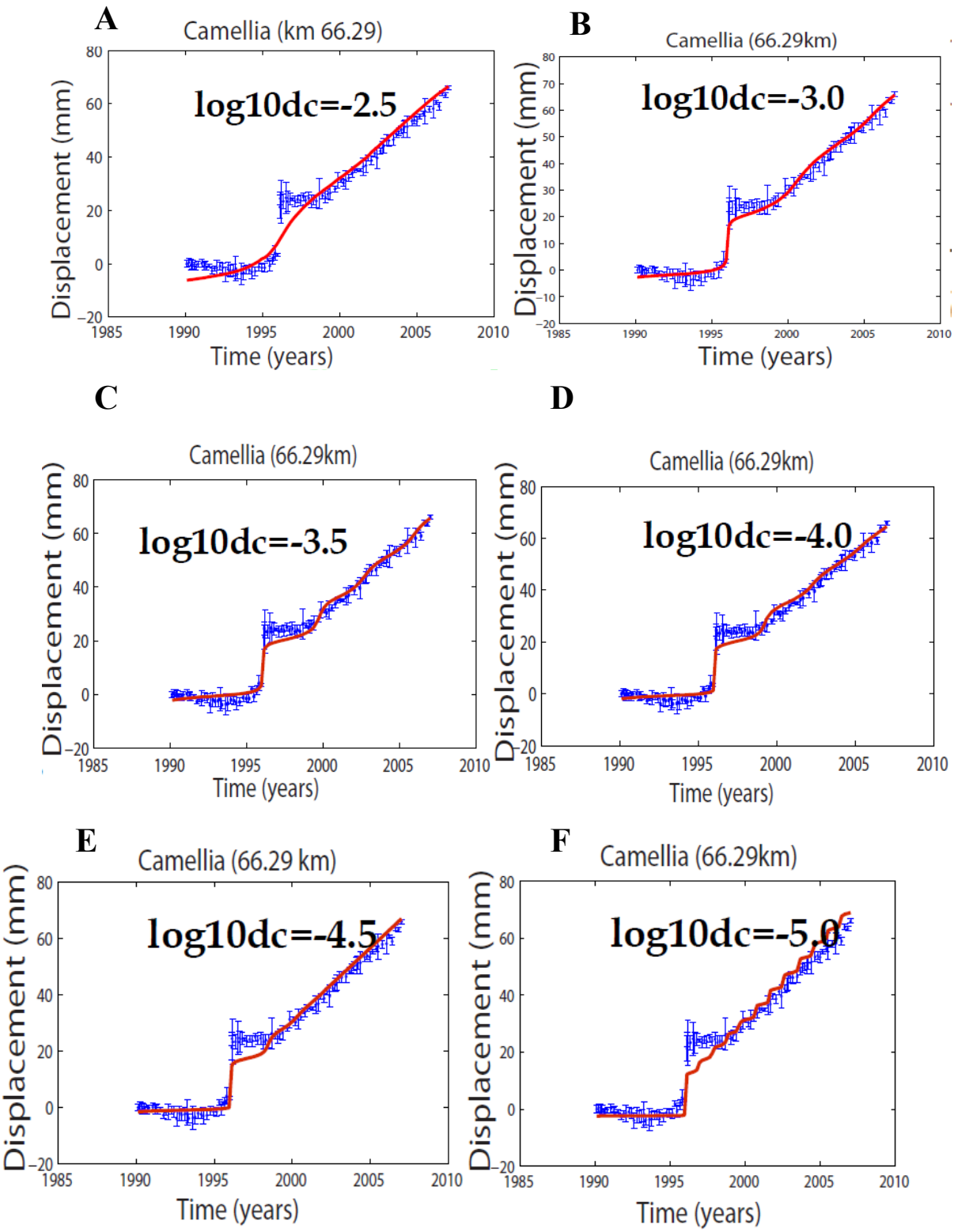

Figure 2.2: Fit to the fault creep data with various fixed d_c values. Red lines are model predicted creep. Blue dots and bars are data and 1σ uncertainties.

Our model places constraints on d_c, the characteristic size of asperities that are required to evolve from one steady state to the other. We run many inversions with various fixed d_c ranging from $10^{-2.5}$ to 10^{-5} m. Figure 2.2 shows model-predicted creep for the Camelia section of the Hayward fault for the various values of d_c. Results show that d_c values greater than 0.001m produce a gradual recovery in creep rate that is entirely inconsistent with observations (Figure 2.2A). However, d_c values smaller than about 10^{-4} reproduce the quiescent creep period and rapid recovery, but the rapid forward creep response ~6 years after the 1989 earthquake is smaller than observed (Figure 2.2E and 2.2F). The small d_c values also produce some oscillations that are not seen in the data (Figure 2.2F). The observations are best reproduced with d_c in the range $10^{-4.5}$ to 10^{-3} m.

The relationship between depth of faulting and spring stiffness is plotted in Figure 2.3. Using the estimated range in elastic stiffness from the spring-slider inversion, we infer that the depth extent of creep is within the range 5.3 km and 7.8 km. This estimate is in reasonable agreement with inferred depth extent of creep on the southernmost Hayward fault by Schmidt et al. [2005] from an inversion of geodetic data (Figure 2.3).

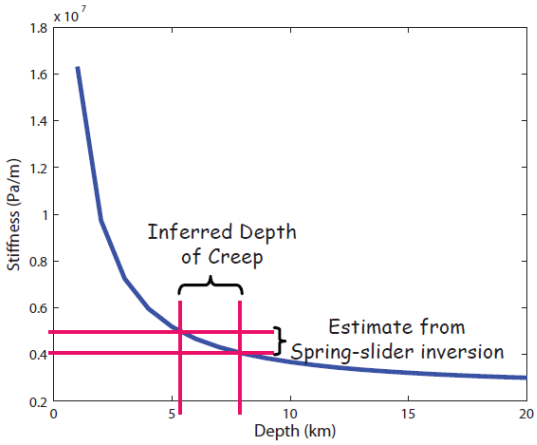

Figure 2.3: Stiffness versus depth computed using a BEM solution for slip on a rectangular fault under uniform stress drop.

The estimate of aσ lies in the range of 0.07 to 0.15 MPa. If we assume typical laboratory values for a of 0.005-0.015 [e.g., *Blanpied, et al* 1998, *Lapusta and Rice,* 2003, *Saffer, et al.,* 2003], we infer effective normal stress on the fault of 5 to 30 MPa. This is lower than the average lithostatic stress of 75-120 MPa over the inferred depth range of creep and is lower than the 50-80 MPa, average effective stress at hydrostatic pore pressure. The small inferred $a\sigma$ could be explained by pore pressure exceeding hydrostatic values, or true friction values smaller than lab values, or both.

The estimate of (a-b)σ lies in the range of $4\text{x}10^{-5}$ to $2.2\text{x}10^{-3}$ MPa. Assuming the inferred range of effective normal stress from the discussion above, the inferred value of *(a-b)* lies between $\sim 1.42\text{x}10^{-6} - 4.45\text{x}10^{-4}$. This is very small. Laboratory measurements show a strong dependence of $a - b$ on temperature, and consequently, depth. *Blanpied et al.* [1995] used experiments on wet granite gouge to infer $a - b$ of order 10^{-3} for temperatures below 400^{o}C and

of order 10^{-2} and increasing roughly linearly with temperature above 400^{o}C. Many numerical simulations adopt a depth distribution of $a-b$ consistent with the laboratory results [e.g., *Lapusta and Rice*, 2003]. Studies utilizing postseismic geodetic data and the velocity strengthening friction law consistently report $(a-b)\sigma$ values in the range 0.2-0.7 MPa [*Hearn et al.*, 2002; *Perfettini and Avouac*, 2004, 2007; *Miyazaki et al.*, 2004; *Hsu et al.*, 2006], which corresponds to $a - b$ of order 10^{-4}–10^{-3} on faults with hydrostatic pore pressure at sub-seismogenic depths.

2.5 3D boundary element models

The spring-slider model is convenient for inversion of data because the forward model is computationally efficient, but it is an obvious oversimplification of creep on the fault. To examine the limitations of the spring-slider model and to examine both the spatial and temporal evolution of creep on the fault, we also set up a boundary element models for the southern section of the Hayward fault. We assume a vertical, planar, 20-km-long fault extending from the ground surface to a depth ranging from 3 to 7 km. The range of model depths is chosen based on a combination of previous studies on the distribution of locking and creep on the Hayward fault (e.g. *Schmidt, et al* 2005) and results from the spring-slider inversion. Using values for friction parameters inferred from the spring-slider inversion, we use the BEM model to solve for the spatial and temporal evolution of the post-1989 creep across the 20 km southernmost section of Hayward fault. We run numerous forward models using various combinations of rate and state frictional parameters $a\sigma$ and $(a-b)\sigma$ within the range of values estimated in our spring-slider inversions. We systematically vary the depth-extent of creep to find values that qualitatively best reproduce the observed displacement time series. For all runs, d_c is 10^{-3} m.

Figure 2.4 shows the spatial and temporal evolution of the creep event. Immediately after the stress change on the fault at t = 1989.79 yr, the creep rate on the fault is reduced everywhere. With time, the fault experiences a gradual creep rate increases from the ends of the fault, especially from the northwestern end while the center region of the fault remains at a low creep rate. Surrounding this central locked section is a ring of high creep rate that begins to close down at year ~1995 and then completely closes at ~1996.18 yr. Following this, a ring of high creep rate expands in radius as creep gradually reduces back to a steady creep rate over the next four years or so. By the year, t = 2002 yr, the fault has nearly returned to each steady-state creep at the long term creep rate.

Figure 2.5 compares the predicted surface creep with the theodolite station measurements using model surface patches nearest to the position of each theodolite station. The parameters producing the fit to the data in Figure 2.5 are as follows: $a\sigma$ = 0.15 MPa, $(a-b)\sigma$ = 0.00013 MPa, α = 0.2, v_1 = 6.7 mm/yr, v_2 = 4.1 mm/yr, and v_3 = 5.3 mm/yr. Figure 2.5 shows that, selecting appropriate model parameters and properties, we are able to explain the general spatial and temporal patterns in creep evolution along the southern section of the Hayward fault.

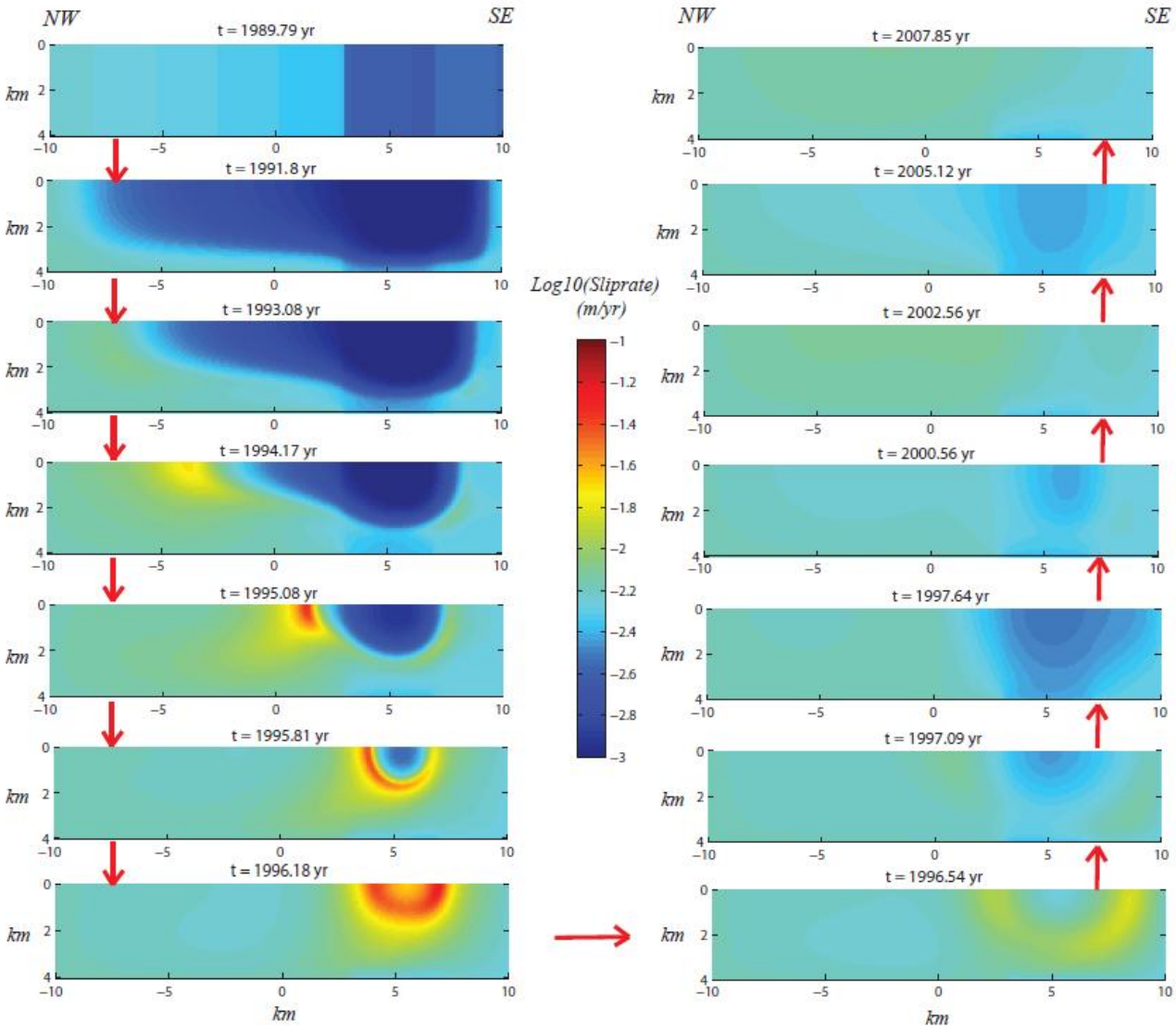

Figure 2.4: Forward modeling of the Southern Hayward creep events (1989 - 2008) using BEM. The red arrows indicate the direction of creep evolution.

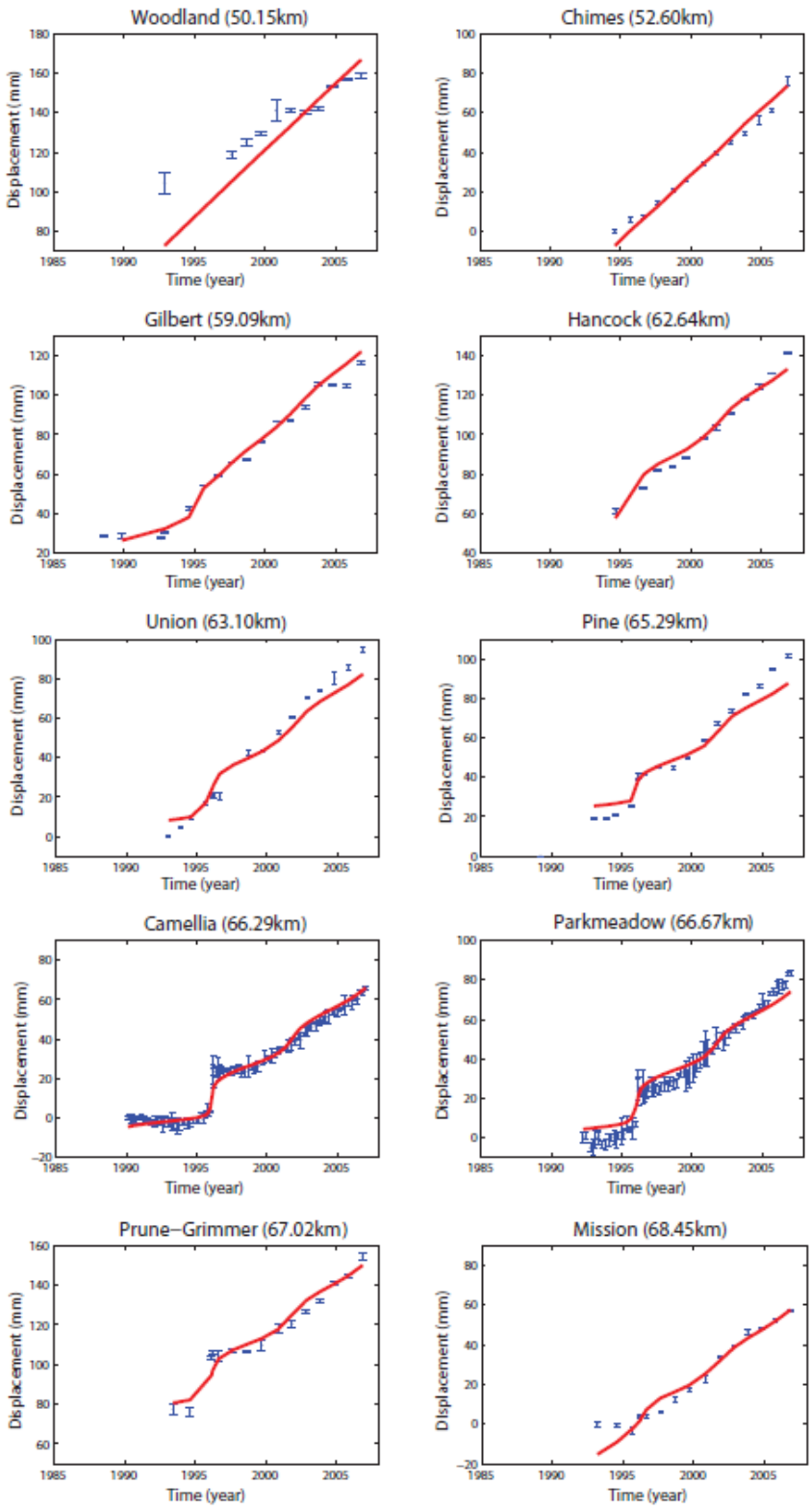

Figure 2.5: BEM forward fitting of Hayward creep measurements (1989-2007). The red lines are the model predicted creep on each of the stations while the blues dots are data measurements. The names of the stations are top of each plot panel.

2.6 Implications for future earthquakes

To examine the implications of the estimated values of friction parameters on the dynamics of fault creep, we simulated earthquake cycles using the numerical model of Segall [2010, p. 352] for a 1D fault in a 2D elastic medium under assumption of antiplane strain. Figure 2.6a shows the 1D BEM model which consists of a 5-km-wide velocity-weakening patch (for earthquake generation) surrounded by velocity-strengthening regions of length 13.5 km (nominally creeping patches). The fault is loaded with steady creep at the ends of the velocity-strengthening regions. We generated earthquake cycle models using two (a-b)σ values: 1.3 x 10^{-4} MPa (similar to inverted values from our spring slider model) and 1.3 x 10^{-1} MPa (consistent with previous afterslip studies mentioned above). Figure 2.6b and 2.6c show the slip evolution on patches shown with red and black squares in Figure 2.6a. Figure 2.6b shows that the response of the creeping patches to earthquakes on the velocity weakening patch (Figure 2.6c) strongly depends on the value of (a-b)σ. In the case of larger (a-b)σ, the velocity-strengthening patch does not slip significantly during the earthquake. The stress induced on the velocity-strengthening patch by the earthquake is released gradually by afterslip resulting in the logarithmic-shaped evolution of slip. In contrast, in the case of small (a-b)σ, the earthquake ruptures through the velocity-strengthening patch resulting in the cosiesmic jump in displacement in Figure 2.6c followed by a period of nearly zero slip and an eventual return to steady sliding. This result suggests that if our inverted values for friction parameters are correct, that earthquakes on locked sections of the Hayward fault might rupture through the creeping areas of fault (at least for the southernmost Hayward where we have the ability to invert for friction parameters).

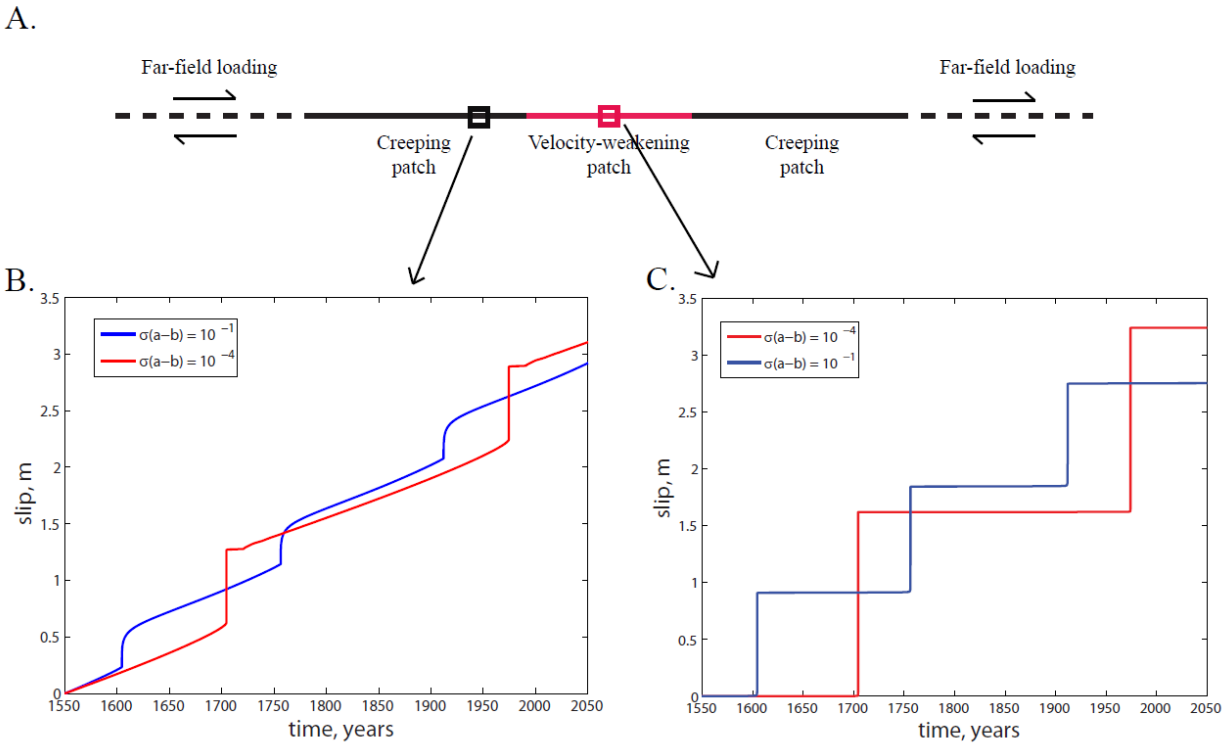

Figure 2.6: Implication of small a-b values. [A] One-dimensional BEM model set-up. The black and red squares are locations for the slip evolution of [B] (creeping patch) and [C] (locked patch) respectively.

Publications resulting from this work

Kanu, C., and K.M. Johnson, Paper #2010JB007927 submitted to Journal of Geophysical Research - Solid Earth (in revision as of Nov. 2010), "Arrest and Recovery of Frictional Creep on the southern Hayward fault triggered by the 1989 Loma Prieta, California earthquake and Implications for Future Earthquakes"

Funning, G., and R. Bürgmann, Paper submitted to Geophysical Research Letters (in revision as of Nov. 2010), "The source region of major earthquakes on the Hayward fault, California"

References

2007 Working Group on California Earthquake Probabilities, The Uniform California Earthquake Rupture Forecast, version 2 (UCERF 2), (2008), (USGS Open File Report 2007-1437, 2008: http://pubs.usgs.gov/of/2007/1437/).

Aagaard, B. T., R. W. Graves, D. P. Schwartz, J. J. Lienkaemper, D. A. Ponce, and R. Graymer (2010a), Ground motion modeling of Haward fault scenario earthquakes I: Construction of the suite of scenarios, Bull. Seismol. Soc. Am., in press.

Aagaard, B. T., et al. (2010b), Ground-motionmodeling of Haward fault scenario earthquakes II: Simulation of long-period and broadband ground motions, Bull. Seismol. Soc. Am., in press.

Bilham, R., S. Whitehead, Subsurface creep on the Hayward fault, Fremont California, Geophys. Res. Lett., 24, 1307-1310 (1997).

Blanchard, F. B., G. L. Laverty, 1966, Displacements in the Claremont Water Tunnel at the intersection with the Hayward fault, Bull. Seismol. Soc. Am., 56, 291-294 (1966).

Blanpied, M. L, Lockner, D. A, Byerlee, J. D., (1995). Frictional slip of granite at hydrothermal conditions. J. Geophys. Res. 100:13045–64

Blanpied, M.L., Marone, C.J., Lockner, D.A., Byerlee, J.D. and King, D.P., (1998). Quantitative measure of the variation in fault rheology due to fluid-rock interactions. Journal of Geophysical Research, 103(B5): 9691-9712.

J. Boatwright, H. Bundock, "Modified Mercalli Intensity maps for the 1868 Hayward earthquake plotted in ShakeMap format" (USGS Open File Report 2008-1121, 2008: http://pubs.usgs.gov/of/2008/1121/)

Bürgmann, R., D. Schmidt, R. M. Nadeau, M. d'Alessio, E. Fielding, D. Manaker, T. V. McEvilly, and M. H. Murray, (2000) Earthquake potential along the northern Hayward fault, California, Science, 289, 1178-1182.

Cluff, L. S., K. V. Steinbrugge, Hayward fault slippage in the Irvington-Niles districts of Fremont, California, Bull. Seismol. Soc. Am., 56, 257-279 (1966).

d'Alessio, M. A. , I. A. Johanson, R. Bürgmann, D. A. Schmidt, M. H. Murray, Slicing up the San Francisco Bay Area: block kinematics and fault slip rates from GPS-derived surface velocities, J. Geophys. Res., 110 (2005), doi:10.1029/2004JB003496.

Ferretti, A., C. Prati, F. Rocca, Permanent scatterers in SAR interferometry, IEEE Trans. Geosci. Remote Sens., 39, 8–20 (2001).

Dieterich, J. H., (1979a) Modeling of rock friction, 1, Experimental results and constitutive equations, J. Geophys. Res., 84, 2161-2168.

Dieterich, J. H., (1979b) Modeling of rock friction, 2, Simulation of preseismic slip, J. Geophys Res.,8 4, 2169-2175.

Fukuda, J., K. M. Johnson, K. M. Larson, and S. Miyazaki (2009), Fault friction parameters inferred from the early stages of afterslip following the 2003 Tokachi-oki earthquake, J. Geophys. Res., 114, B04412, doi:10.1029/2008JB006166.

Graymer, R. W. et al., Three-dimensional geologic map of the Hayward fault, northern California: Correlation of rock units with variations in seismicity, creep rate, and fault dip, Geology, 33, 521-524 (2005).

Hearn, E. H., R. Bürgmann, and R. E. Reilinger (2002), Dynamics of I ̇zmit earthquake postseismic deformation and loading of the Du ̈zce earthquake hypocenter, Bull. Seismol. Soc. Am., 92, 172–193, doi:10.1785/0120000832.

Hsu, Y., Simons, M., Avouac, J., Galetzka, J., Sieh, K., Chlieh, M., Natawidjaja, D., Prawirodirdjo, L. & Bock, Y., (2006). Frictional afterslip following the 2005 Nais-Simeulue earthquake, Sumatra, Science, 312, doi:10.1029/2003JB002917, 1921–1926.

Johanson, I.A., E. J. Fielding, F. Rolandone, R. Bürgmann, Coseismic and postseismic slip of the 2004 Parkfield earthquake from space-geodetic data, Bull. Seismol. Soc. Am., 96, S269-S282 (2006).

Johnson, K.M., R. Bürgmann, and K. Larson, 2006. Frictional properties on the San Andreas Fault near Parkfield, California, Inferred from Models of Afterslip following the 2004 Earthquake. Bulletin of the Seismological Society of America, Vol. 96, No. 4B, pp. S321-S338, doi: 10.1785/0120050808.

Johnson, K., Bürgmann, R and Freymueller, J. T. (2009). Coupled afterslip and viscoelastic flow following the 2002 Denali Fault, Alaska earthquake. Geophys. J. Int. 176, 670–682

Langbein, J., J. R. Murray, H. A. Snyder, Coseismic and initial postseismic deformation from the 2004 Parkfield, California, earthquake, observed by Global Positioning System, electronic distance meter, creepmeters and borehole strainmeters, Bull. Seismol. Soc. Am., 96, S304-S320 (2006).

Lapusta, N. and J. R. Rice, (2003). Nucleation and early seismic propagation of small and large events in a crustal earthquake model, J. Geophys. Res. 108, doi:10.1029/2001JB000793..

Lienkaemper, J.J., J.S. Galehouse, and R.W. Simpson, (1997) Creep response of the Hayward fault to stress changes caused by the Loma Prieta earthquake, Science, 276, 2014-2016.

Lienkaemper, J. J., J. S. Galehouse, and R. W. Simpson, (2001) Long-term monitoring of creep rate along the Hayward fault and evidence for a lasting creep response to 1989 Loma Prieta earthquake, Geophys. Res. Lett., 28, 2265– 2268.

Lienkaemper, J. J., P. L. Williams, A record of large earthquakes on the southern Hayward fault for the past 1800 years, Bull. Seismol. Soc. Am., 97, 1803-1819 (2007).

Malservisi, R., C. Gans, K. P. Furlong, Numerical modeling of creeping faults and implications for the Hayward fault, California, Tectonophysics, 361, 121-137 (2003).

McFarland, F.S., J. J. Lienkaemper, S. J. Caskey, “Data from theodolite measurements of creep rates on San Francisco Bay region faults, California: 1979-2009”, (USGS Open-File Report 2009-1119, 2009: http://pubs.usgs.gov/of/2009/1119/)

Murray, J. R., J. Langbein, Slip on the San Andreas fault at Parkfield, California over two earthquake cycles and the implications for seismic hazard, Bull. Seismol. Soc. Am., 96, S283-S303 (2006).Ruina, A. L. (1983), Slip instability and state variable friction laws, J. Geophys. Res., 88, 10,359– 10,370.

Saffer, D. M., and C. Marone, (2003). Comparison of Smectite and Illite Frictional Properties: Application to the Updip Limit of the Seismogenic Zone Along Subduction Megathrusts, Earth and Planetary Science Letters, 215, 219-235, 2003.

Schmidt, D. A., R. Bürgmann, R. M. Nadeau, and M. d'Alessio (2005), Distribution of aseismic slip rate on the Hayward fault inferred from seismic and geodetic data, J. Geophys. Res., 110, B08406, doi:10.1029/2004JB003397.

Schmidt, D. A., and R., Bürgmann, (2008) Predicted reversal and recovery of surface creep on the Hayward fault following the 1906 San Francisco earthquake, Geophys. Res. Lett., 35.

Segall, P. (2010). Earthquake and Volcano deformation. Princeton University Press. New Jersey, USA. p. 364 – 366.

Simpson, R. W. , J. J. Lienkaemper, J. S. Galehouse, Variations in creep rate along the Hayward fault, California, interpreted as changes in depth of creep, Geophys. Res. Lett., 28, 2269-2272 (2001).

Thomas, A.L., 1993. Poly3D : a three-dimensional, polygonal element, displacement discontinuity boundary element computer program with applications to fractures, faults, and cavities in the Earth's crust, M.S.; 221 p., Stanford University.

Yu, E., P. Segall, Slip in the 1868 Hayward earthquake from the analysis of historical triangulation data: J. Geophys. Res., 101, 16,101–16,118 (1996).